0.6–3-GHz Wideband Receiver RF Front-End With a Feedforward Noise and Distortion Cancellation Resistive-Feedback LNA

Xiao Wang, Johannes Sturm, Na Yan, Xi Tan, and Hao Min

Abstract—A novel wideband receiver RF front-end, including a resistive negative feedback wideband low-noise amplifier (LNA) with feedforward noise and distortion cancellation and a current commutating down conversion passive mixer with biquad trans-impedance amplifier, is presented in this paper. In comparison to conventional resistive negative feedback LNAs, theory analysis and experimental results for the proposed LNA circuit shows improved performance parameters, including voltage gain, noise figure (NF), and input-referred third-order intercept point (IIP3), especially helpful for wideband LNA design in modern deep-submicrometer CMOS. A wideband receiver RF front-end fabricated in 0.13-μm CMOS, based on the proposed feedforward noise and distortion-cancellation resistive-feedback LNA, has 42–48-dB conversion gain with 0.8–12-MHz tunable IF -3-dB bandwidth and 12-dB adjacent channel selectivity at $2f_p$, -14-dBm IIP3, and 3-dB NF double-sideband with 10-kHz flicker-noise corner frequency.

Index Terms—Noise cancellation, RF front-end, wideband.

I. INTRODUCTION

WITH THE exploding growth of the wireless communication markets, feature-rich mobile handsets need to support more and more communication standards, as well as reduced power consumption and cost. Thus, multimode transceivers, software-defined radios (SDRs), and cognitive radios have generated significant interest in academic and industry research. One of the most challenging problems for SDR application is an RF front-end that satisfies all the specifications of various communication standards.

Using the f_T advantage of the scaling-down CMOS processes, a wideband RF front-end can cover the frequency range from 50 MHz to several gigahertz with an acceptable dynamic range performance, which makes it a promising solution for SDR and multimode receiver application. Compared with the multimode receiver with multiple narrowband low-noise amplifier (LNA) arrays, the coilless wideband front-end also has the benefit of less magnetic mutual coupling and much less chip area occupation for low-cost system-on-chip (SOC) design.

However, there are also several challenging design issues for wideband receiver front-end design, such as the bandwidth (related to f_T of the specific process), voltage gain, and linearity, limited by scaling-down power-supply voltage and the noise figure (NF) with increasing thermal noise coefficient of the scaling-down CMOS.

In this paper, a novel feedforward noise- and distortion-cancellation technique is proposed to combine the resistive negative-feedback and noise-cancellation technique to improve the performance of a wideband LNA. Analysis shows that compared to conventional resistive negative-feedback LNAs, the voltage gain, NF, and input-referred third-order intercept point (IIP3) are significantly improved, especially for wideband LNA design in the scaling-down deep-submicrometer CMOS process. Based on the proposed novel LNA structure, a 0.6–3-GHz wideband RF front-end, including a pseudodifferential wideband LNA and in-phase/quadrature (I/Q) current commuting passive mixer with programmable bandwidth second-order trans-impedance amplifier (TIA), is implemented in 0.13-μm CMOS for multimode receiver application.

The proposed negative feedback and feedforward noise-canceling operation principle is presented in Section II. The detailed analysis of LNA parameters is also presented to show performance improvement compared to conventional structures. Section III presents details of the current commutating passive mixer design. Section IV presents the RF front-end test-chip design and measurement results. Finally, a conclusion is summarized in Section V.

II. WIDEBAND LNA

NF, which determines the receiving sensitivity, is one of the key characteristics for wireless receivers. However, limited by the wideband input impedance matching, the NF performance of a wideband LNA is not as good as narrowband LNAs. In recent years, several techniques, such as feedback [1], [2], [4] and noise cancellation [3], have been investigated to break or alleviate the tradeoff between wideband input impedance matching and NF. Shunt–shunt feedback can be used to adjust the input impedance and improve NF. Negative feedback decreases the input impedance for common-source amplifiers, while positive
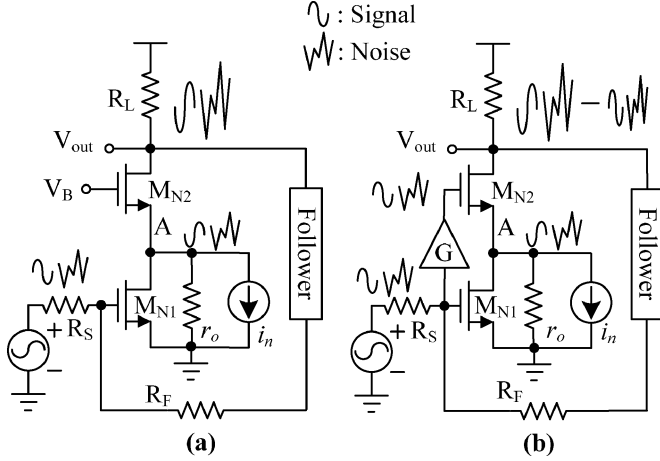
Fig. 1.   (a) Conventional resistive-negative-feedback LNA. (b) Proposed resistive-negative-feedback LNA with feedforward noise and distortion cancellation.

feedback [4] increases input impedance for common gate amplifiers. For the noise-cancellation technique, the key idea is to use an additional auxiliary amplifier, which senses the signal and noise voltage and combining the outputs of the main and the auxiliary amplifier such that noise from the input device cancels while signal contributions are added at the output node.

Fig. 1(a) presents the schematic of a conventional resistive-negative-feedback LNA, which is widely used in recently reported studies [1], [2]. M_{N1} is the transconductance transistor and constant biased M_{N2} is a cascode transistor to increase the output impedance and improve the isolation between input and output ports. R_L is the load resistor. The current source i_n models the channel thermal noise source of M_{N1}, which is the main noise contributor to the overall NF, and r_o models the drain output impedance of M_{N1}. M_{N1}, M_{N2}, R_L, and the follower work as a common-source inverse amplifier, which composes the "ideal" amplifier with high input impedance and low output impedance. The feedback resistor R_F is determined by the input impedance matching as

$$R_F = R_S(1 + |A_V|) \tag{1}$$

where R_S is the source impedance (50/75 Ω) and A_V is the voltage gain of the common-source amplifier.

By investigating the signal and noise voltage polarities of all nodes (input, output, node A) in Fig. 1(a), the signal voltage polarity of the input port and node A is inverted, while the noise voltage polarity is the same. Therefore, an extra signal and noise path can be introduced to realize a noise-canceling technique in the resistive-negative-feedback LNA.

As presented in Fig. 1(b), a positive gain stage G is introduced to amplify the signal and noise at the input port to the gate of cascode transistor M_{N2}. As the noise voltage polarity at the gate and the source of M_{N2} is the same, the noise voltage between the gate and source of M_{N2} decreases, and therefore the noise current flowing through load R_L at the output also decreases, which means noise cancellation. The noise-canceling condition is

$$V_{in,n} \times G(f) = V_{A,n} \tag{2}$$

where $V_{in,n}$ and $V_{A,n}$ is the noise voltage at the input port and node A, respectively. However, when gain G increases, $V_{in,n}$ decreases and $V_{A,n}$ increases because of the negative feedback loop. For perfect noise canceling according (2), an infinite gain G would be necessary, which is not practical for circuit design, but a finite gain G still helps to cancel a significant part of the noise, as revealed in the following analysis.

The signal voltage between the gate and source of M_{N2} increases with lower output impedance of M_{N1}, which generally uses the minimum channel length for wideband design. Therefore, with the help of extra gain stage G, the output signal current will increase and the voltage gain will be enhanced. The gain enhancement is determined by the gain G and the output impedance of M_{N1}. The main performance parameter of this proposed LNA is analyzed as follows.

A. Voltage Gain

The overall transconductance G_m of the LNA is defined by an equivalent transconductance G_{m1} of transistor M_{N1} and G_{m2} of transistor M_{N2}. M_{N1} works as a common-source amplifier including cascode M_{N2} with

$$G_{m1}(f) = g_{m1}(f) \times \frac{g_{m2}(f) \times r_0(f)}{1 + g_{m2}(f) \times r_0(f)} \tag{3}$$

where g_{m1} and g_{m2} are the transconductance of M_{N1} and M_{N2}, respectively, and r_0 is the output resistance of M_{N1}. M_{N2} works as a source degenerated common-source amplifier where the source resistor is just the output impedance r_0 of M_{N1}. Taking gain G into account, the effective transconductance of M_{N2} is

$$G_{m2}(f) = \frac{G(f) \times g_{m2}(f)}{1 + g_{m2}(f) \times r_0(f)}. \tag{4}$$

The overall voltage gain is

$$A_V = -(G_{m1} + G_{m2}) \times R_L. \tag{5}$$

Compared to the conventional structure shown in Fig. 1(a), which corresponds to $G = 0$, the voltage gain is enhanced by

$$\alpha = \frac{G_{m2}}{G_{m1}} \times 100\% = \frac{G(f)}{g_{m1}(f) \times r_0(f)} \times 100\%. \tag{6}$$

The gain enhancement α is the ratio of gain G and intrinsic gain $g_{m1}r_0$ of M_{N1}. Therefore, this proposed feedforward technique can take advantage of the decreasing single transistor intrinsic gain in deep-submicrometer CMOS processes in order to improve the overall LNA gain.

B. Input Impedance Matching

As the proposed feedforward technique is part of the whole negative feedback loop, it does not change the essence of the equivalent input impedance. Therefore, the feedback resistor R_F still satisfies (1). The only difference to the conventional structure is that the gain A_V is enhanced by α, and R_F should rise accordingly.

C. NF

The NF is analyzed under the precondition of input impedance matching. Gain stage G is treated as a noiseless ideal device (as shown in Section II-E, gain stage G is
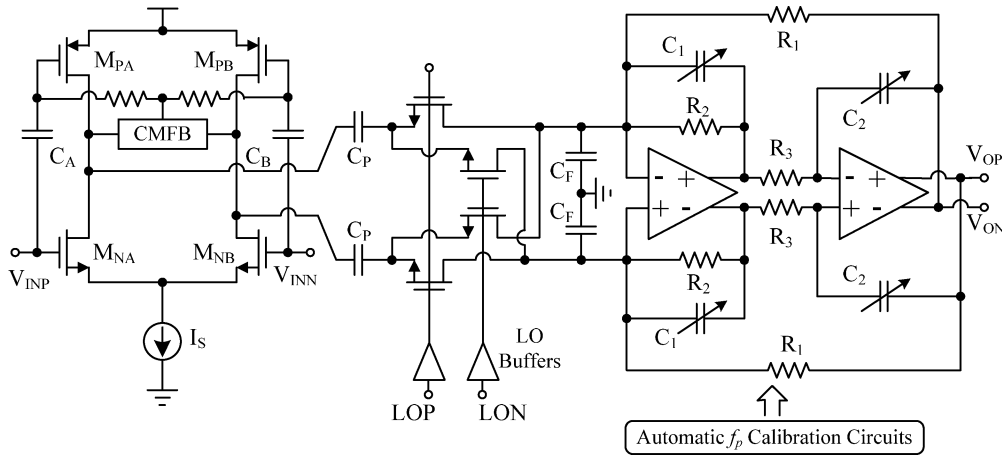
Fig. 2. F_{M1} improvement versus G and MOS intrinsic gain.

implemented by noiseless passive devices). Since the channel thermal noise source i_n is the main noise contributor to the output noise voltage, the contribution of i_n is carefully analyzed (the other contributors would be analyzed afterwards). The equivalent input and output noise voltage satisfies

$$V_{\text{in},n} = \frac{1}{2 - A_V} V_{\text{out},n}. \tag{7}$$

By solving the noise current equation at node A, the noise contribution of i_n to the overall output noise voltage is

$$V_{\text{out},n} = \frac{A_V}{2} \left(1 + \frac{1}{1 - A_V} \right) \times \frac{i_n}{g_{m1}(1 + \alpha)}. \tag{8}$$

The contribution of i_n to the overall noise factor is

$$F_{M1} = \frac{V_{\text{out},n}^2}{A_V^2 \times 4KTR_S}$$
$$= \left(1 + \frac{1}{1 - A_V} \right)^2 \frac{\gamma}{4g_{m1}R_S(1 + \alpha)^2} \tag{9}$$

where γ is the MOS transistor thermal noise coefficient. F_{M1} can be improved by increasing α since both the α and the voltage gain A_V is part of the denominator in (9). Therefore, the proposed noise-canceling technique helps to decrease the noise contribution of transistor M_{N1}.

Fig. 2 presents the F_{M1} improvement of the proposed circuit, compared to conventional resistive-negative-feedback wideband LNA. The noise improvement gets more dominant for modern CMOS technologies since the intrinsic gain decreases with the minimum channel length (about 15 dB/18 dB/20 dB for 65-nm/90-nm/130-nm CMOS, respectively).

The proposed negative-feedback LNA with a feedforward noise-canceling technique helps to reduce the main noise contribution of M_{N1}. When taking all the noise contributions of M_{N2}, R_L, R_F into account, the overall noise factor is

$$F = 1 + \left(1 + \frac{1}{1 - A_V} \right)^2$$
$$\times \frac{\gamma}{4R_S(1 + \alpha)^2} \left[\frac{1}{g_{m1}} + \frac{1}{g_{m2}(g_{m1}r_0)^2} \right]$$
$$+ \frac{R_S}{4R_F} + \frac{R_L}{4R_S(1 - A_V)^2}. \tag{10}$$

Fig. 3. Schematic of the proposed pseudodifferential wideband LNA.

Due to the voltage gain enhancement and feedforward noise-canceling technique, the noise contribution of M_{N2}, R_L, R_F, and the follower can also be reduced as gain is enhanced.

D. Distortion

By using Taylor approximation of the drain current, the non-linear high-order terms can be modeled as a current source in parallel with M_{N1}. Therefore, distortion components are also cancelled by the same mechanism as noise canceling.

Furthermore, the voltage swing at node A decreases as gain G increases, thus the distortion component of M_{N1} introduced by velocity saturation and channel length modulation can be decreased.

E. Proposed LNA Implementation

Based on the proposed feedforward noise- and distortion-cancellation resistive-feedback LNA, a pseudodifferential wideband LNA (shown in Fig. 3) is implemented in the 0.13-μm CMOS process. The input signal is converted to differential by an off-chip balun with 1:4 impedance ratio and the LNA is matched internally to 200 Ω, which provides 5–6-dB voltage gain and improves the overall NF, but degrades the linearity and bandwidth. The signal and noise at differential input ports is directly coupled to the gate of M_{N2} to realize gain of feedforward path $G \approx 1$, without extra power consumption, noise, distortion, and phase shift. Therefore, it satisfies the precondition of noiseless ideal component in the part of NF analysis in Section II-C.

M_{P1} provides part of the dc-bias current flowing through M_{N1} to reduce the voltage drop across R_L. The input signal is ac coupled to the gate of M_{P1}, enhancing the transconductance to improve gain and NF. M_{N3} and M_{N4} are implemented as a source follower to buffer the feedback resistor R_F. Simulation results show that with the $G = 1$ feedforward directly coupling ($\alpha \approx 10\%$–15%), in comparison with the conventional resistive-feedback structure, the NF and voltage gain are improved by 0.3 and 1–2 dB, respectively.

Fig. 4. Schematic of the current commutating passive mixer.

III. CURRENT COMMUTATING PASSIVE MIXER

A current commutating passive mixer, which has the superior advantage of low flicker noise and high linearity with low power supply voltage [9], [10], is applied here to handle strong interference, and to relax the design tradeoff between low-frequency flicker noise and wide channel bandwidth for a multimode receiver with various IF bandwidth requirement.

As shown in Fig. 4, a current reuse transconductor converts the input signal to RF current and then feeds the double-balanced passive current commutating mixer. The bias voltage of M_{PA} and M_{PB} is generated by common-mode feedback circuits, and the parasitic capacitor at the output nodes of transconductor is optimized as small as possible to increase the output impedance, for the purpose of improving the NF [9]. The mixing switches, which are biased in the ON overlap region for linearity performance, are driven by inverter-type local oscillator (LO) buffers.

A Tow–Thomas biquad is applied to realize the tunable bandwidth TIA and filters part of the out-of-band interference. In comparison with the conventional single-pole output TIA, biquad introduces more noise, which degrades the NF of the mixer; furthermore, the increased out-of-band input impedance of the biquad decreases the out-of-band IIP3 of the mixer. On the other hand, the biquad helps to relax the linearity requirement of the following stages such as the low-pass filter (LPF) and variable gain amplifier (VGA), and thus improve the linearity of the overall receiver chain by 5–6 dB, especially for low power-supply voltage design. A current-mode class-AB operational transconductance amplifier (OTA) with 400-MHz unit gain bandwidth, as presented in Fig. 5, is used in the biquad to guarantee the out-of-band linearity. The output node with large capacitance loading is designed as the dominant pole, and the poles at internal nodes are pushed larger that 1.2 GHz to guarantee the stability.

R_1, R_3, C_1, and C_2 have the same value for relaxing the bandwidth tuning complexity, and the cutoff frequency is given by

$$f_p = \frac{1}{2\pi\sqrt{R_1 R_3 C_1 C_2}} = \frac{1}{2\pi R_1 C_1}. \tag{11}$$

Resistors and capacitors are tuned by switches to choose the responding bandwidth in the wide IF frequency range of
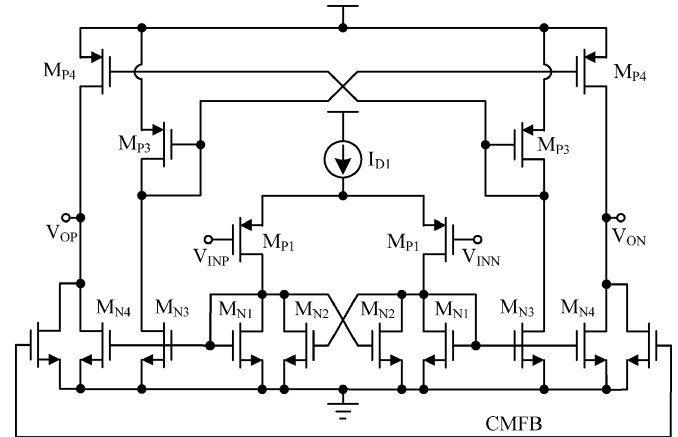

Fig. 5. Schematic of the current-mode class—AB OTA.

0.8–12 MHz. Limited by the tradeoff between the conversion gain and high linearity requirement of this mixer, resistor R_1 is typically 1–2 kΩ, capacitance of C_1 and C_2 are as large as 8 pF for 12-MHz high bandwidth in this design and 120 pF for 0.8-MHz low bandwidth. For saving the chip area, MOS capacitors are used in the loop instead of metal–insulator–metal (MIM) capacitors, at the expense of 0.5-dB linearity degradation due to the nonlinearity of varactors. An automatic f_p calibration loop is added to calibrate the PVT variation and keeps f_p within ±2% accuracy.

IV. WIDEBAND RF FRONT-END IMPLEMENTATION AND MEASUREMENT RESULTS

Based on the proposed feedforward noise-cancellation resistive-feedback wideband LNA and current commutating passive mixer, the wideband RF front-end testchip, with I/Q IF output, is fabricated in 0.13-μm CMOS, as shown in Fig. 6. It occupies a chip area of 1 mm × 1.5 mm, including the pad ring for measurement. The chip is assembled by a chip-on-board (COB) package for measurement. I/Q LO signals are generated by an on-chip low-noise divider. Noise contributed by LO phase noise can be neglected and analyzed from simulation results.

Fig. 7 presents the measured $S11$ from 500 MHz to 3 GHz. The $S11$ achieves <-15-dB matching around 1.5 GHz, but
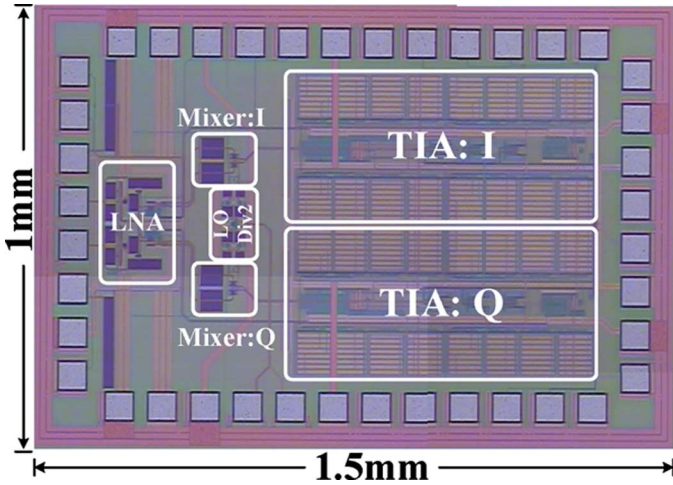
Fig. 6. Microphotograph of the wideband RF front-end testchip.
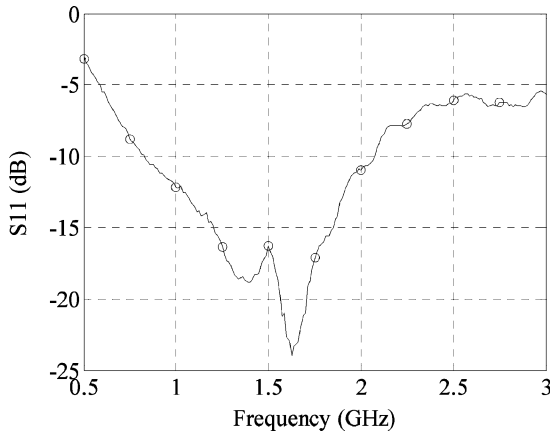
Fig. 7. Measured $S11$.
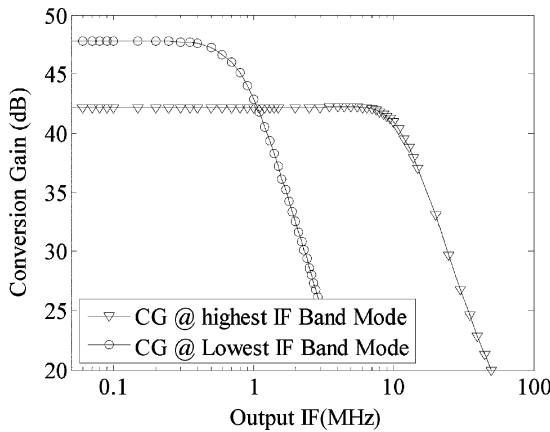
Fig. 8. Conversion gain under various bandwidth configurations.
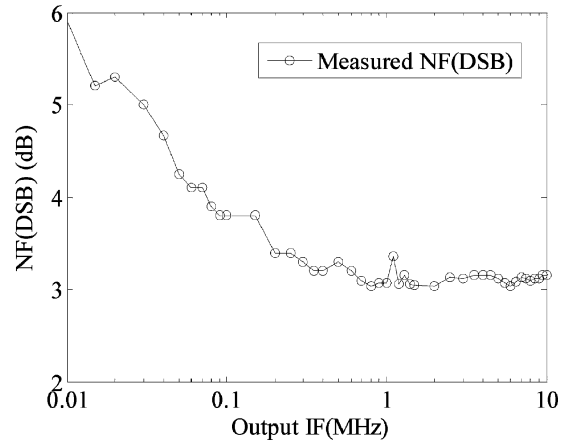

Fig. 9. Measured NF DSB.

Fig. 10. Measured IIP3.

TABLE I
OVERVIEW OF WIDEBAND RF FRONT-END

	THIS WORK	**[6]**	**[7]**
CMOS	**0.13μm**	0.13μm	65nm
RF Band	**0.6~3GHz**	0.3~2.6GHz	2.1~8.2GHz
Output IF	**0.8~12MHz with 0.8MHz tuning step**	1~5MHz	--
Gain	**48~42dB 12dB ACS@2f_p**	38dB	20dB
NF(DSB)	**3dB**	3.6dB	5.85dB
IIP3	**-14dBm**	-6.5dBm* 4dBm#	>-12dBm
S11	**<-8dB**	<-10dB	<-10dB
Area	**1.5mm²**	**2.25mm²**	**0.21mm²**
Supply	**1.2V**	**1.5V**	**1.2V**
Power	**30mW**	52.5mW	47mW

*nominal   #manually tuned

shows degradation at a higher frequency due to the limited frequency range (nominal 0.6–3-GHz range from the datasheet) of the off-chip wideband balun. The conversion gain under lowest and highest output IF bandwidth configuration is presented in Fig. 8. The conversion gain reaches 42–48 dB at 2.2-GHz RF frequency band (including about 4–5-dB voltage gain of the 1:4 impedance ratio off-chip balun). The tunable IF bandwidth covers 0.8–12-MHz frequency range with 0.8-MHz linear

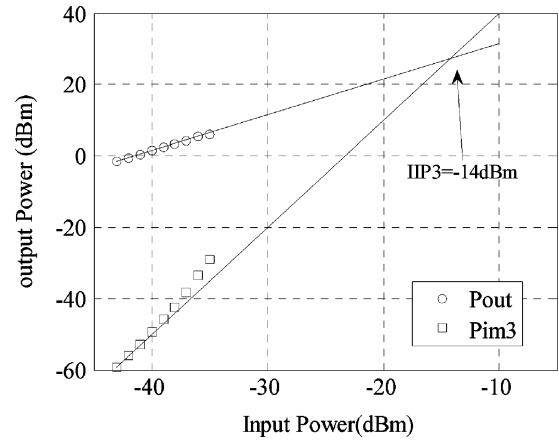tuning steps. The low-pass biquad TIA provides 12-dB ACS at 2 f_p, thus decreases the linearity requirement of the following stages, and also provides a solution for high-gain RF front-end design with low power-supply voltage. The double-sideband

(DSB) NF is 3 dB with 10-kHz flicker-noise corner frequency, as presented in Fig. 9, and loss from the balun (about 0.4–0.5 dB) has been deembeded in measurement results. The IIP3 reaches -14 dBm with 1.5- and 1.501-GHz two-tone measurement (Fig. 10). The performance summary and the comparison with previously reported results are presented in Table I. This work achieves high gain, low noise, high linearity, and wide frequency tuning-range IF output, while the 30-mW (including the LO divider and buffers) power consumption is reasonably low.

V. CONCLUSION

A wideband receiver RF front-end with feedforward noise and a distortion-cancellation resistive-feedback LNA has been presented in this paper. Experimental results validate that this technique improves the NF, gain, and linearity of the resistive-feedback LNA, especially for LNA design in scaling down deep-submicrometer CMOS. The wideband receiver RF front-end achieves high gain, low noise, and high linearity, and also provides effective adjacent channel selection to relax the following stages.

REFERENCES

[1] J. Borremans, S. Thijs, M. Dehan, A. Mercha, and P. Wambacq, "Low-cost feedback-enabled LNAs in 45 nm CMOS," in *Proc. IEEE Eur. Solid-State Circuits Conf.*, Sep. 2009, pp. 100–103.

[2] J.-H. C. Zhan and S. S. Taylor, "A 5 GHz resistive-feedback CMOS LNA for low-costmulti-standard applications," in *Int. Solid-State Circuits Conf. Tech. Dig.*, 2006, pp. 721–730.

[3] F. Bruccoleri, E. A. M. Klumperink, and B. Nauta, "Wide-band CMOS low-noise amplifier exploiting thermal noise canceling," *IEEE J. Solid-State Circuits*, vol. 39, no. 2, pp. 275–281, Feb. 2004.

[4] A. Liscidini *et al.*, "A 0.13 μm CMOS front-end, for DCS1800/UMTS/ 802.11b-g with multiband positive feedback low-noise amplifier," *IEEE J. Solid-State Circuits*, vol. 41, no. 4, pp. 981–989, Apr. 2006.

[5] J. Borremans, P. Wambacq, C. Soens, Y. Rolain, and M. Kuijk, "Low-area active-feedback low-noise amplifier design in scaled digital CMOS," *IEEE J. Solid-State Circuits*, vol. 43, no. 11, pp. 2422–2433, Nov. 2008.

[6] N. Poobuapheun, W. Chen, Z. Boos, and A. M. Niknejad, "An inductorless high dynamic range 0.3–2.6 GHz receiver CMOS front-end," in *Proc. IEEE Radio Freq. Integr. Circuits Symp.*, 2009, pp. 397–390.

[7] S. K. Hampel, O. Schmitz, M. Tiebout, and I. Rolfes, "Wideband inductorless minimal area RF front-end," in *Proc. IEEE Eur. Solid-State Circuits Conf.*, Sep. 2009, pp. 96–99.

[8] X. Wang, W. Aichholzer, and J. Sturm, "A 0.1–4 GHz resistive feedback LNA with feedforward noise and distortion cancellation," in *Proc. IEEE Eur. Solid-State Circuits Conf.*, Sep. 2010, pp. 406–409.

[9] S. Chehrazi *et al.*, "Noise in current-commutating passive FET mixers," *IEEE Trans. Circuits Syst. I, Reg. Papers*, vol. 57, no. 2, pp. 332–344, 2010.

[10] V. Giannini *et al.*, "A 2-mm 2 0.1–5 GHz software-defined radio receiver in 45-nm digital CMOS," *IEEE J. Solid-State Circuits*, vol. 44, no. 12, pp. 3486–3498, Dec. 2009.

[11] J. Borremans *et al.*, "Low-area active-feedback low-noise amplifier design in scaled digital CMOS," *IEEE J. Solid-State Circuits*, vol. 43, no. 11, pp. 2422–2433, Nov. 2008.

[12] H. Darabi and A. A. Abidi, "Noise in RF-CMOS mixers: A simple phsical model," *IEEE Trans. Solid-State Circuits*, vol. 35, no. 1, pp. 15–25, Jan. 2000.

[13] W.-H. Chen *et al.*, "A highly linear broadband CMOS LNA employing noise and distortion cancellation," *IEEE J. Solid-State Circuits*, vol. 43, no. 5, pp. 1164–1176, May 2008.

Xiao Wang, photograph and biography not available at time of publication.

Johannes Sturm, photograph and biography not available at time of publication.

Na Yan, photograph and biography not available at time of publication.

Xi Tan, photograph and biography not available at time of publication.

Hao Min, photograph and biography not available at time of publication.